Draft version June 12, 2013
Preprint typeset using LaTeX style emulateapj v. 11/10/09

EQUATION OF STATE EFFECTS ON THE MINIMUM CORE MASS FOR GIANT PLANET FORMATION

Ana-Maria A. Piso
Harvard-Smithsonian Center for Astrophysics

Andrew N. Youdin
JILA, University of Colorado at Boulder

Ruth A. Murray-Clay
Harvard-Smithsonian Center for Astrophysics
Draft version June 12, 2013

ABSTRACT

The core accretion model assumes that giant planets form through gas accretion on to a solid core. The core and the atmosphere initially grow simultaneously through stages of quasistatic equilibrium; once the core becomes massive enough, the atmosphere is no longer in hydrostatic balance and a rapid phase of runaway gas accretion commences. The minimum core mass for which unstable atmosphere collapse occurs is typically called the "critical core mass". In standard calculations of the critical core mass, planetesimal accretion dominates the atmosphere evolution, and the energy deposited by incoming planetesimal on to the core is radiated away by the atmosphere. In this study we consider a low planetesimal accretion regime in which the luminosity evolution of the atmosphere is dominated by Kelvin-Helmholtz contraction. We use the atmosphere structure and cooling model developed in Piso & Youdin (in prep.) to derive the profile and evolution of atmospheres composed of a gas described by a realistic equation of state. We find that the minimum core mass (which we denote as *critical core mass*) to form a giant planet before the dissipation of the protoplanetary disk is substantially increased compared to an ideal gas polytrope when non-ideal effects such as hydrogen dissociation and ionization are taken into account. Moreover, our results yield lower mass cores than corresponding studies for large planetesimal accretion rates. We therefore show that it is easier to form a planet by growing the core first, then accreting a massive gaseous envelope, rather than forming the core and atmosphere simultaneously.

1. INTRODUCTION

One of the prevalent theories of giant planet formation is the core accretion model (Mizuno et al. 1978, Stevenson 1982, Bodenheimer & Pollack 1986, Wuchterl 1993, D'Angelo et al. 2011). In this model, a solid core is first formed; the core grows, and once it becomes large enough it can accumulate a massive atmosphere. In the standard core accretion models, the atmosphere is heated due to accretion of planetesimals, and as a result it radiates away energy. The envelope is therefore in a steady state at all times, and the atmosphere mass is a function of the core mass. It is thus found that there exists a minimum core mass past which hydrostatic equilibrium breaks down and rapid, unstable gas accretion commences: this is called the "critical core mass".

However, the planetesimal accretion rate is not necessarily constant at a given location in the protoplanetary disk throughout the disk lifetime (e.g., Ikoma et al. 2000). If the planetesimal accretion rate is very low, the atmosphere can no longer gain energy due to accretion of solids, and is instead dominated by gas accretion, contracting on a Kelvin-Helmholtz timescale. In Piso & Youdin (in prep.) we studied the formation of giant planet atmospheres under the assumption that Kelvin-Helmoholtz gas contraction dominates the luminosity evolution of the atmosphere over planetesimal accretion. We built quasi-static two-layer atmosphere models with an inner convective region and an outer radiative region that matches smoothly onto the protoplanetary disk. We derived a cooling model to connect series of quasi-static atmospheres, and thus obtained an evolutionary history of the envelope. We defined the time at which unstable atmosphere collapse commences as the crossover time $t_{\rm co}$, at which $M_{\rm atm}(t_{\rm co}) \sim M_{\rm c}$. From this we defined as *critical core mass* the minimum core mass for a protoplanet to initiate runaway gas accretion during the lifetime of the protoplanetary disk. We studied this minimum mass for a variety of disk conditions, nebular gas compositions and opacities. We found that the critical core mass decreases for larger stellocentric distances, and is smaller for lower disk temperatures and opacities and for a higher mean molecular weight of the gas.

Piso & Youdin (in prep.) assume that the nebular gas can be described by a polytropic equation of state (EOS) corresponding to an ideal diatomic gas: $\nabla_{\rm ad} = 2/7$. In reality, however, non-ideal effects, such as gas dissociation and ionization, have to be taken into account. A realistic hydrogen-helium mixture can be described using tabulated equation of state tables. In this study, we use the Saumon et al. (1995) EOS tables to describe the nebular gas. We generate atmosphere profiles and estimate atmospheric cooling timescales for a variety of disk conditions. From this, we determine the minimum core mass required for runaway gas accretion to commence within the typical life timescale of the protoplanetary disk. We

find that the realistic equation of state yields larger critical core masses compared to the ideal gas polytrope.

This paper is organized as follows. In section 2 we review the quasi-static and evolution models derived in Piso & Youdin (in prep.). We discuss the variations in the adiabatic gradient, and hence in the atmosphere structure, caused by a non-ideal equation of state in section 3, and discuss the implications of this variability on the atmosphere evolution time in section 4. We determine the minimum core mass to form a giant planet during the disk lifetime when the nebular gas is described by a realistic equation of state in section 5. In section 6 we compare our results to similar results obtained in studies that consider planetesimal accretion as the dominant source of energy. Finally, we summarize our findings in section 7.

2. MODEL REVIEW

In this section we review the model developed in Piso & Youdin (in prep.) for the structure and evolution of a planetary atmosphere embedded in a protoplanetary disk. We describe the assumptions of the model and the properties of our assumed protoplanetary disk in section 2.1, and we summarize the equations describing the structure and time evolution of a static atmosphere in section 2.2.

2.1. *Assumptions and Disk Model*

We assume that the planet consists of a solid core of fixed mass and a two-layer atmosphere composed of an inner convective zone and an outer radiative zone that matches smoothly on to the disk. The two regions are separated by the Schwarzschild criterion for convective instability. We denote the surface between the two regions as the radiative-convective boundary (RCB), which is henceforth defined by a radius $r = R_{\rm RCB}$. The evolution of the atmosphere is dominated by Kelvin-Helmholtz contraction rather than planetesimal accretion, and the luminosity is assumed to be constant throughout the outer radiative region. The atmosphere is considered to be spherically symmetric and self-gravitating. It consists of a hydrogen-helium mixture, with hydrogen and helium mass fractions of 0.7 and 0.3, respectively. We further assume that the envelope evolves through stages of quasi-static equilibrium.

As a fiducial disk model, we use the minimum mass, passively irradiated model of Chiang & Youdin (2010). In this model, the surface density and mid-plane temperature are given by

$$\Sigma_{\rm d} = 2200 F_\Sigma a^{-3/2} \text{ g cm}^{-2} \quad (1a)$$

$$T_{\rm d} = 120 F_T a^{-3/7} \ K, \quad (1b)$$

with a the semi-major axis in AU, and F_Σ and F_T normalization factors that adjust the disk mass and temperature relative to the minimum mass solar nebula (MMSN). In this study, we assume $F_\Sigma = F_T = 1$. The resulting mid-plane pressure is given by

$$P_{\rm d} = 110 F_\Sigma \sqrt{F_T m_*} a^{-45/14} \text{ dyn cm}^{-2} \quad (2)$$

for a mean molecular weight $\mu = 2.35$. Here $m_* \equiv M_*/M_\odot$, where M_* is the mass of the central star and $M_\odot$ is the mass of the Sun. We choose $m_* = 1$.

2.2. *Structure Equations and Cooling Model*

An atmosphere in hydrostatic equilibrium is described by the following structure equations:

$$\frac{dP}{dr} = -\frac{Gm}{r^2}\rho \quad (3a)$$

$$\frac{dm}{dr} = 4\pi r^2 \rho \quad (3b)$$

$$\frac{dT}{dr} = \nabla \frac{T}{P}\frac{dP}{dr} \quad (3c)$$

$$\frac{dL}{dr} = 4\pi r^2 \rho \epsilon_g, \quad (3d)$$

where r is the radial coordinate, P, T and ρ are the gas pressure, temperature and density, respectively, m is the mass enclosed by the radius r, L is the luminosity from the surface of radius r, and $\epsilon_g \equiv -T\frac{ds}{dt}$ represents the heating per unit mass due to gravitational contraction, with s the specific gas entropy. The temperature gradient $\nabla \equiv \frac{d\ln T}{d\ln P}$ has different expressions depending on the primary means of energy transport throughout the atmosphere. We assume that energy can be transported either through radiation or convection. When the luminosity is carried by radiative diffusion, the temperature gradient is given by

$$\nabla = \nabla_{\rm rad} \equiv \frac{3\kappa P}{64\pi G m \sigma T^4} L, \quad (4)$$

where σ is the Stefan-Boltzmann constant and κ is the opacity. Alternatively, when the energy is transported outwards through convective motions, the temperature gradient becomes

$$\nabla = \nabla_{\rm ad} \equiv \Big(\frac{d\ln T}{d\ln P}\Big)_{\rm ad}, \quad (5)$$

where $\nabla_{\rm ad}$ is the adiabatic temperature gradient. The process that dominates energy transport throughout the atmosphere is determined by the Schwarzschild criterion (e.g., Thompson 2006): the atmosphere is stable against convection when

$$\nabla < \nabla_{\rm ad} \quad (6)$$

and convectively unstable when the reverse is true. In order for convection to be effective, $\nabla \approx \nabla_{\rm ad}$. Therefore, we find that the temperature gradient is given by $\nabla = \min(\nabla_{\rm ad}, \nabla_{\rm rad})$.

In order for equation set (3) to be solvable, it has to be supplemented by an equation of state (EOS) that relates pressure, temperature and density $P = P(\rho, T)$, and an opacity law for κ. In this study we use the interpolated EOS tables of Saumon et al. (1995) for a helium fraction $Y = 0.3$. More details on the EOS tables and the methodology of combining the separate tables for hydrogen and helium are presented in section 3 and Appendix A.

We assume an opacity power law of the form

$$\kappa = \kappa_0 \Big(\frac{P}{P_{\rm ref}}\Big)^\alpha \Big(\frac{T}{T_{\rm ref}}\Big)^\beta, \quad (7)$$

with α, β, κ_0 constants, and $T_{\rm ref}$ and $P_{\rm ref}$ a normalizing temperature and pressure, respectively. To estimate α, β and κ_0 we use the Bell & Lin (1994) opacity laws for ice grains: $\alpha = 0$, $\beta = 2$ and $\kappa_0 = 2$. We note that these values are valid only for low disk temperatures: $T_d \lesssim 100K$. As such, we only consider cool atmospheres that form in the outer part of the protoplanetary disk ($a \geq 5$ AU).

We now discuss our choice of core parameters and boundary conditions. We assume a solid core of fixed mass M_c with a radius $R_{\rm c} = (3M_{\rm c}/4\pi\rho_{\rm c})^{1/3}$, where $\rho_{\rm c}$ is the core density. We choose $\rho_{\rm c} = 3.2$ g cm^{-3} (e.g., Papaloizou & Terquem 1999). Furthermore, we assume the atmosphere matches on to the protoplanetary at a distance equal to its Hill radius, the distance at which the gravitational attraction of the planet and of the host star are comparable. Its radius is given by

$$R_{\rm H} \equiv a\Big(\frac{M_{\rm p}}{3M_\odot}\Big)^{1/3} \tag{8}$$

Outside the Hill radius, the gravity of the planet is overcome by the tidal gravity from its host star, and hence only gas that lies within the Hill sphere can be gravitationally bound to the planet. We choose the effective outer boundary of the atmosphere to be the surface defined by the Bondi radius. The Bondi radius represents the distance from the planet at which the thermal energy of the nebular gas is of the order of the gravitational energy binding the gas to the planet. It is defined as

$$R_{\rm B} \equiv \frac{GM_{\rm p}}{c_s^2} = \frac{GM_{\rm p}}{\mathcal{R}T_{\rm d}}, \tag{9}$$

where G is the gravitational constant, $M_{\rm p}$ is the total mass of the planet, c_s is the sound speed, and $\mathcal{R}$ is the reduced gas constant: $\mathcal{R} = k_b/(\mu m_p)$, with k_b the Boltzmann constant and m_p the proton mass. Outside the Bondi sphere, the core gravity is too weak to significantly affect the nebular gas, justifying the choice of Bondi radius as the relevant scale for the atmosphere. We note that the Hill radius is still the correct scale for matching on to the disk, as perturbations of the nebular gas still occur past the Bondi radius due to the gravitational influence of the core. The above choice for the atmosphere boundary is only applicable when the Bondi radius is smaller than the Hill radius. If, on the other hand, $R_{\rm B} > R_{\rm H}$, the atmosphere only extends out to the Hill radius, since material cannot be gravitationally bound to the protoplanet outside the Hill sphere. At the Hill radius, the temperature and pressure are given by the nebular temperature and pressure: $T(R_{\rm H}) = T_{\rm d}$ and $P(R_{\rm H}) = P_{\rm d}$. For a given core mass, the atmosphere profile and evolution are therefore uniquely determined by the outer boundary conditions.

Lastly, we review the cooling model developed in Piso & Youdin (in prep.) used to determine the time evolution of the atmosphere between subsequent static models. A protoplanetary atmosphere embedded in a gas disk satisfies the following cooling equation:

$$L = L_c + \Gamma - \dot{E} + e_{\rm acc}\dot{M} - P_M\frac{\partial V_M}{\partial t} \tag{10}$$

This cooling model applies at any radius R where the mass enclosed is M, for example the Bondi radius, the Hill radius, or the radius of the radiative-convective boundary. L is the total luminosity, $L_{\rm c}$ is the luminosity from the solid core, and may include planetesimal accretion and radioactive decay. Γ is the heat generation rate, $\dot{E}$ is the rate at which total energy (internal and gravitational) is lost, and $e_{\rm acc}$ is the specific total energy brought in by mass accreting at the rate $\dot{M}$: $e_{\rm acc} = u - GM/R$. The last term represents the work done on a surface mass element.

As a consequence of the equations above, both the atmosphere structure and the gas accretion rate are uniquely determined by the current atmosphere mass. As this mass accretion rate is slow compared to the time it takes to relax to this solution, we can make a quasi-static model of the atmosphere growth. By connecting sets of subsequent static atmospheres through the cooling equation (10) we can obtain an evolutionary atmosphere series.

3. ADIABATIC GRADIENT FOR THE TABULATED EQUATION OF STATE

In this section we explain the differences in the behavior of thermodynamic variables between an ideal gas polytrope and a realistic equation of state by studying the dependence of the adiabatic gradient (defined in equation 5) on temperature and pressure. Figure 1 shows a contour plot of the adiabatic gradient as a function of gas temperature and pressure, which was obtained by interpolating and extending the Saumon et al. (1995) equation of state tables as referenced in section 2 and described in Appendix A.

We distinguish three separate temperature regimes:

1. Intermediate temperature regime (300 K $\lesssim T \lesssim$ 3000), where the hydrogen-helium mixture behaves as an ideal gas characterized by a polytropic equation of state.

2. High temperature regime ($T \gtrsim 3000$ K), where dissociation of molecular hydrogen occurs, followed by ionization of atomic hydrogen.

3. Low temperature regime ($T \lesssim 300$ K), where the temperature becomes low enough for rotational motion to reduce.

We note that helium behaves like an ideal monatomic gas in our regime of interest ($\nabla_{\rm ad} = 2/5$). As such, its presence in the atmosphere only causes a small, constant upper shift in the adiabatic gradient of the mixture.

In what follows we explain the behavior of the adiabatic gradient in the three temperature regimes separately.

1. Intermediate T: Ideal Gas

For temperatures less than ~ 2000 K but larger than ~ 300 K, the hydrogen molecule is not energetic enough to dissociate and hydrogen behaves as an ideal diatomic gas. We see this in Fig. 1 for 300 K $\lesssim T \lesssim$ 3000 K, where the adiabatic gradient is approximately constant. The helium component of the gas causes a slight increase in the adiabatic index: $\nabla_{\rm ad} \approx 0.3$ in this temperature range rather than 2/7 as is the case for a diatomic gas.

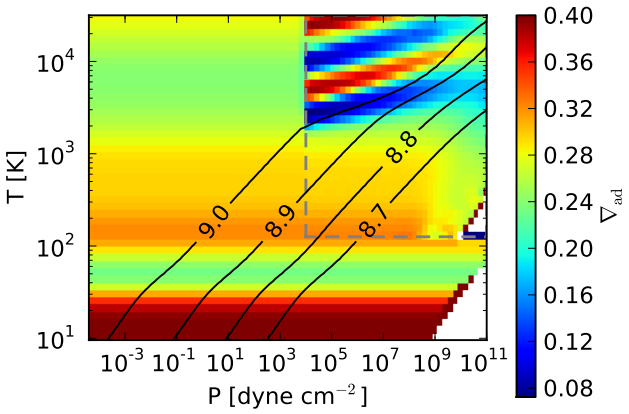

FIG. 1.— Contour plot of the adiabatic gradient ∇_{ad} for a hydrogen-helium mixture as a function of gas temperature and pressure. The upper right rectangle encloses the region described by the original Saumon et al. (1995) EOS tables, while the rest of the plot is our extension to lower temperatures and pressures. The black curves represent constant entropy adiabats, with the labels the natural logarithm of the absolute entropy per unit mass. At high temperatures, hydrogen dissociates and ionizes, while at low temperatures the rotational states of the hydrogen molecule are only partially excited and it therefore no longer behaves like an ideal diatomic gas. The discontinuity between the original EOS tables and our extension is due to the fact that we did not take into account dissociation and ionization. However, in our regime of interest (encompassed by the constant entropy curves), the extension matches smoothly with the original tables.

2. High T: Dissociation and Ionization of Hydrogen.

At low temperatures, hydrogen exists in molecular form, which has a stable configuration. As the temperature becomes higher than $T \sim 2000 - 3000$ K, the internal energy becomes large enough to break the covalent bond between the atoms, and hydrogen starts dissociating. At temperatures of the order of 10^4 K, the internal energy becomes large enough to remove electrons from the atoms, and hydrogen ionizes. In stellar and giant planet interiors there is little overlap between the two processes: hydrogen is almost entirely dissociated into atoms by the time ionization becomes important.

For a mixture of molecular and atomic hydrogen, we expect the adiabatic gradient to have an intermediate value between monatomic and diatomic gas, while for a mixture of protons and electrons the adiabatic index is just 2/5 as for a monatomic ideal gas. However, we notice in Fig. 1 that the adiabatic gradient decreases significantly in the regions where hydrogen is either partially dissociated or partially ionized. We further explain this behavior.

We first discuss ionization. For a mixture of ideal gases, the total internal energy is given by the sum of the internal energies of the individual gases. When a gas is ionized, however, the energy used to ionize the atoms has to also be taken into account. This energy depends on the ionization fraction and can be determined from the Saha equation (see e.g., Kippenhahn & Weigert 1990). The ionization fraction only depends on gas temperature and density (see Appendix B), and hence only the equation of state. An expression of the adiabatic gradient as a function of the ionization fraction can be derived. We present this expression in Appendix B. The adiabatic gradient is $\nabla_{ad} = 2/5$ when there is no ionization (i.e., only atomic hydrogen) or when the plasma is fully ionized, but decreases significantly during partial ionization, reaching a minimum when half of the gas is ionized.

This is consistent with the behavior we see in Figure 1. At constant entropy, we expect an increase in pressure to increase the internal energy of the system, thus causing the temperature to also rise significantly. In the case of partial ionization, however, part of the internal energy is used to remove the electrons from atoms, and therefore there is less energy available to increase the temperature of the system. This behavior of the constant entropy curves is seen in Figure 1.

The dissociation of molecular hydrogen is dictated by an equation similar to the Saha equation, with the ionization energy replaced by dissociation energy (equal to 4.27 eV for molecular hydrogen, Mandl 1989). The adiabatic gradient therefore has an analogous behavior, consistent with Fig. 1.

3. Low T: Hydrogen Rotation and Spin Isomers

As a diatomic molecule, hydrogen has five degrees of freedom, three associated with translational motion and two associated with rotation. At room temperature, the rotational states are fully excited and the full rotational effects are seen. The excitation temperature for rotation is $\Theta_r \approx 85$ K for the hydrogen molecule (e.g., Kittel et al. 1981); as the gas temperature becomes comparable to Θ_r, fewer rotational states are excited and rotation entirely ceases as $T \to 0$.

In this section we discuss the quantum effects of the hydrogen isomeric forms and the way they affect the rotational energy and heat capacity of the hydrogen molecule at low temperatures, and hence the adiabatic gradient.

Molecular hydrogen occurs in two isomeric forms: orthohydrogen, with parallel proton spins, and parahydrogen, with antiparallel proton spins. The Pauli exclusion principle requires the total wavefunction of two fermions, such as protons, to be antisymmetric. As such, a symmetric spin wavefunction requires an antisymmetric rotational wavefunction, and vice-versa (Farkas 1935). Parahydrogen has an antisymmetric spin wavefunction, which means that it can only occupy symmetric rotational states and hence the angular quantum number j has to be even. By analogy, orthohydrogen must have an antisymmetric rotational wavefunction and can only occupy states with odd j. The partition functions for ortho- and parahydrogen are described in Appendix A. At equilibrium, the relative abundance of the ortho and para states is given by the ratio of their partition functions. For very low temperatures there is only parahydrogen, as molecules are in the ground state with $j = 0$, which corresponds to the para state. As the temperature is increased, parahydrogen starts converting into orthohydrogen, resulting in an ortho-para equilibrium ratio of 3:1 at room temperature.

The internal energy and specific heat per unit mass associated with rotation for the individual isomers and for the equilibrium mixture can be derived from equations (A5), (A6), (A7), (A11) and (A13) and plotted in Figure 2. The para state has no rotational energy for low tem-

peratures, since all the molecules occupy the rotational level with $j = 0$. Orthohydrogen, on the other hand, is in the $j = 1$ state, and so has an energy given by the energy of its first rotational level. Since all the hydrogen mixtures behave like monatomic gases at low temperatures, their rotational heat capacity is zero in this region. This is consistent with $\nabla_{\rm ad} = 2/5$ at low temperatures as seen in Fig. 1. There are two significant maxima in the heat capacities of parahydrogen and of the mixture. At very low temperatures, the heat capacity of parahydrogen is zero because only the lowest accessible energy level $j = 0$ is occupied and a temperature increase does not provide enough energy to populate the next higher level. When the temperature becomes sufficiently high to populate the second lowest level $j = 2$, the heat capacity rapidly increases, passes through a maximum and starts to decrease when the second lowest level becomes saturated. The maxima in the ortho-para mixture appears around the time when parahydrogen starts converting into orthohydrogen. The heat capacity of the equilibrium mixture is not a weighted average of the heat capacities of the individual components because it takes into account both the rotational energy uptake of para- and ortho-hydrogen, and also the shift in their equilibrium concentrations with temperature. At $T = 0$, only parahydrogen is present in the equilibrium mixture; as the temperature is increased, the energetically higher-lying ($j = 1$) ortho-hydrogen is formed, and the concomitant energy increase is seen as a peak in the heat capacity. As the adiabatic gradient is inversely proportional to the heat capacity, it means that the former has to first decrease from 2/5 as the temperature increases, reach a minimum around 50 K ($\nabla_{\rm ad} \approx 0.25$ from Fig. 1), then gradually increase to 2/7 as for a diatomic gas. This behavior is illustrated in Fig. 1.

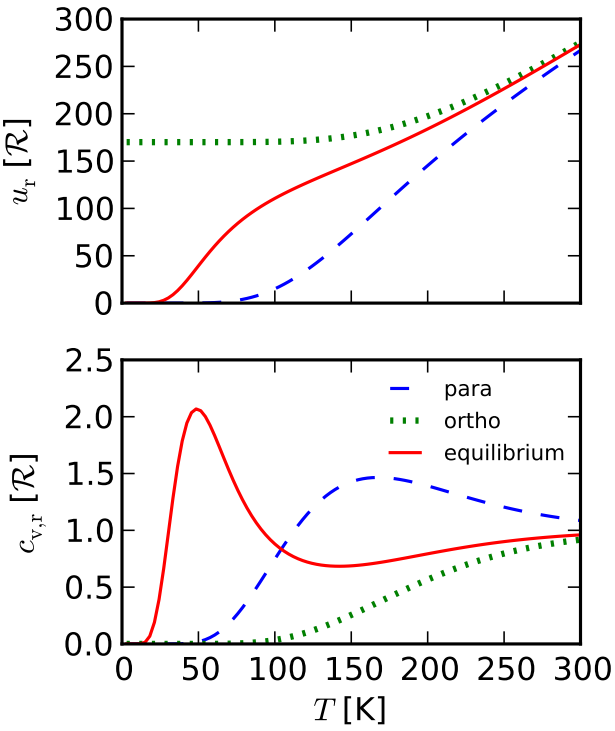

FIG. 2.— Internal energy and heat capacity per unit mass for the hydrogen spins isomers and the equilibrium mixture as a function of temperature.

4. EQUATION OF STATE EFFECTS ON ATMOSPHERE EVOLUTION

Variations in the adiabatic gradient have two competing effects on the atmosphere evolution: they affect the luminosity of the envelope and the amount of energy needed to accrete more mass, i.e. dE/dM. Together, they result in changes in the growth time of the atmosphere, and therefore in the crossover time and critical core mass. In this section we discuss how the variable adiabatic gradient discussed in section 3 affects the atmosphere evolution when compared to an ideal gas of constant $\nabla_{\rm ad}$. We explore the effect of partial dissociation and hydrogen spin isomers (see section 3) on the atmosphere luminosity and cooling time evolution. As the adiabatic gradient is variable throughout the atmosphere profiles described in section (**some previous section**), we first investigate the differences in atmosphere profiles and evolution for ideal gas polytropes with different adiabatic gradients in section 4.1. We then show how the variable adiabatic gradient affects the time evolution of the atmosphere in section 4.2.

4.1. *Ideal Gas Polytropes with Different Adiabatic Gradient*

In this section we investigate the differences in luminosity and dE/dM, and the resulting time evolution, between ideal gas polytropes with different adiabatic gradients: $\nabla_{\rm ad} = 2/7$ (diatomic gas) and $\nabla_{\rm ad} = 2/5$ (monatomic gas). We assume both gases have the same mean molecular weight.

We generate atmosphere profiles for the two different adiabatic indices at $a = 10$ AU and for a core mass $M_{\rm c} = 10 M_{\oplus}$, and estimate the luminosity and cooling time evolution as described in section 2. The results are shown in Figure 3. We find that the polytrope with the lower adiabatic gradient has both a higher luminosity and a longer cooling time. We use instantaneous atmosphere profiles to explain these effects.

We first discuss the effect of the variable adiabatic gradient on luminosity. Figure 4, top panel, shows the temperature profile as well as the location of the radiative-convective boundary for the two polytropes at a fixed total mass $M_{\rm tot} = 11.8 M_{\oplus}$. The polytrope with a larger adiabatic gradient has a more shallow convective zone, and hence a deeper radiative region, since a larger temperature gradient delays the onset of convection. As the luminosity in the radiative region is inversely proportional to the depth of the radiative zone (see equation (3d)), a deeper radiative region results in a lower luminosity, which explains the results in the top panel of Figure 3.

We study the energy behavior for the two polytropes in order to explain the dE/dM effect. We have shown in Piso & Youdin (in prep.) that polytropes with $\nabla_{\rm ad} = 2/7$ have most of the energy concentrated at the bottom of the atmosphere, while polytropes with $\nabla_{\rm ad} = 2/5$ have the bulk of the energy towards the outer boundary. The bottom panel of Figure 4 shows an instantaneous energy

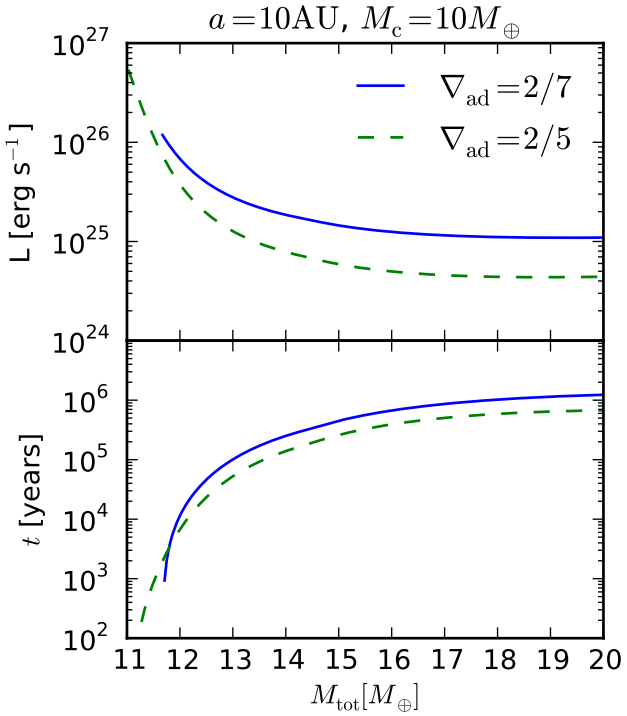

FIG. 3.— Luminosity and time evolution as a function of total mass (core + atmosphere) for polytropes with different adiabatic indices, for a planet forming at 10 AU and with a fixed core mass $M_c = 10M_\oplus$. A larger adiabatic index results in both a lower luminosity and a shorter cooling time.

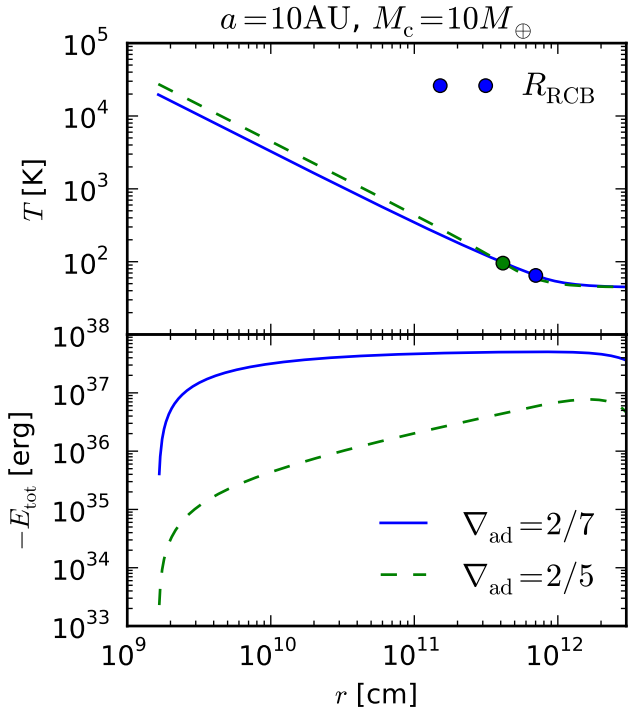

FIG. 4.— Instantaneous temperature and total energy profiles as a function of radius for polytropes with different adiabatic indices, for a planet forming at 10 AU and with a fixed core mass $M_c = 10M_\oplus$. The total mass (core + atmosphere) is $11.8M_\oplus$. The location of the radiative-convective boundary is marked. A lower adiabatic gradient results in a more shallow radiative region (upper panel), and in the total energy being concentrated at the bottom of the atmosphere (lower panel).

profile for the same total mass $M_{tot} = 11.8M_\oplus$, confirming this behavior. It takes more energy to bring in gas deep in the atmosphere for an envelope that has the bulk of its energy concentrated towards the bottom, resulting in a larger dE/dM. The energy effect prevails over the luminosity effect, resulting in a longer cooling time for the envelope, as shown in the bottom panel of Figure 3.

4.2. *Dissociation and Spin Isomers Effects*

We now discuss the differences in luminosity and dE/dM between an ideal gas with constant adiabatic gradient and atmospheres with variations in ∇_{ad} as prescribed by the equation of state discussed in section 4. In what follows we describe our choices of equation of state combinations. From the adiabatic gradient table shown in Figure 1 we find that ∇_{ad} has the flattest behavior around $T = 500$ K. In this region, the gas behaves like an ideal gas with constant polytropic index $\nabla_{ad} \approx 0.3$, with the shift from diatomic gas caused by the helium in the mixture. We generate three sets of atmosphere profiles. The first one corresponds to an ideal gas of constant adiabatic index $\nabla_{ad} = 0.3$. The second one is described by the real EOS for temperatures larger than 500 K and by an ideal gas with $\nabla_{ad} = 0.3$ for $T < 500$ K. Finally, the third profile consists of an ideal gas polytrope with $\nabla_{ad} = 0.3$ for $T > 500$ K and a real gas in the low temperature regime. We compare the first two profiles to show the dissociation effects, and the first and third profile to show the effects of ortho- and parahydrogen. The resulting time evolution is shown in Figure 5.

We see that both dissociation and spin isomers have a comparable effect on the atmosphere growth, and result in slower cooling, and therefore a longer crossover time, when compared to the polytropic ideal gas equation of state. The cooling time is dependent on both the total energy released due to the contraction of the envelope and the luminosity of the atmosphere. In what follows we explore the relative influence of these two factors separately.

The right panel of Figure 6 shows the luminosity evolution with mass for the three combinations of equations of state described above, as well as for the complete real gas EOS. We use again instantaneous atmosphere profiles to explain the differences. The left panel of Figure 6 shows the instantaneous temperature profile and the location of the radiative-convective boundary for a total fixed mass $M_{tot} = 11.8M_\oplus$. The real equation of state for low temperatures is characterized by a lower adiabatic index in the outer regions, due to the spin effects, and is therefore dominant in the radiative zone. As a result, it generates a deeper radiative zone with a lower luminosity, which explains the results in the left panel of Figure 6. Moreover, since the cooling time is inversely proportional to the luminosity, the spin effect will result in a longer cooling (and crossover) time.

The energy behavior is shown in Figure 7. The real EOS for high temperatures has a low adiabatic index deep in the atmosphere, due to hydrogen dissociation,

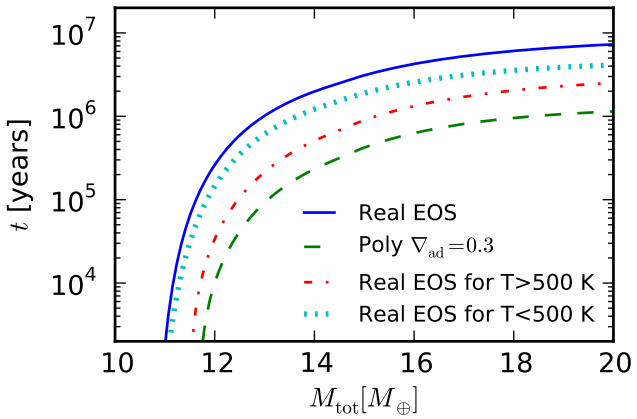

FIG. 5.— Cooling time evolution as a function of total mass (core + atmosphere) for a variety of EOS combinations, for a planet forming at 10 AU and with a fixed core mass $M_{\rm c} = 10M_\oplus$. The cooling time is larger both due to hydrogen dissociation and spin effects when compared to an ideal gas polytrope.

and thus the bulk of its energy concentrated at the bottom of the atmosphere, for the reasons described in section 4.1. It takes more energy to add mass more mass deep in the atmosphere, and dE/dM is larger as a result.

We have seen that the spin effect at the outer boundary dictates the location of the radiative zone, and therefore the luminosity behavior, while dissociation deep in the atmosphere dictates the energy behavior. Overall, both effects result in a longer time for the atmosphere to evolve.

5. CRITICAL CORE MASS

In this section we put together the results obtained in section 4 and determine the minimum core mass to initiate runaway gas accretion during the lifetime of the protoplanetary disk assuming that the nebular gas is described by a realistic equation of state as prescribed by the Saumon et al. (1995) EOS tables (see section 4). As in Piso & Youdin (in prep.), we define this minimum core mass as the *critical core mass*. Moreover, we define the time elapsed until runaway gas accretion is initiated when $M_{\rm atm} \sim M_{\rm c}$ as the *crossover time*. In this section we first explore the dependence of the crossover time on the core mass for a fixed semi-major axis. We then determine the critical core mass to form a giant planet before the dissipation of the gas in the protoplanetary disk, assuming that the nebular gas is described by a realistic hydrogen-helium mixture, and we compare this with the results from Piso & Youdin (in prep.) for an ideal diatomic gas.

Figure 8 displays the time evolution and the crossover time for core masses between 7 and 16 $M_\oplus$ at $a = 10$ AU in our fiducial disk. The crossover time is shorter for lower mass cores, consistent with the results of Piso & Youdin (in prep.).

Figure 9 shows the critical core mass for a massive atmosphere to form during a typical lifetime of a protoplanetary disk $t = 3$ Myrs, for a gas described by a realistic equation of state. For comparison, we also plot the results of Piso & Youdin (in prep.) for an ideal diatomic gas. The use of a realistic equation of state increases the critical core mass by more than a factor of 2. As such, non-ideal effects substantially affect the core mass needed to form a giant planet before the dissipation of the protoplanetary disk.

6. MODEL RELEVANCE IN PLANET FORMATION THEORY

In this study we have considered atmospheres for which planetesimal accretion is negligible and Kelvin-Helmholtz contraction dominates the luminosity evolution of the atmosphere. This is different from standard calculations, in which the atmosphere is heated by planetesimal accretion. In this section we compare our results for the critical core mass to analogous results from the standard calculations. We discuss the core accretion rates that are necessary for our regime to be valid in section 6.1. We then compare our results with planetesimal accretion results under similar assumptions in section 6.2.

6.1. *Planetesimal Accretion Rates*

We estimate the planetesimal accretion rate consistent with our assumptions that $L_{\rm acc} \ll L_{\rm KH}$. Here $L_{\rm acc}$ is the accretion luminosity given by

$$L_{acc} = G\frac{M_{\rm c}\dot{M}_{\rm c}}{R_{\rm c}}, \tag{11}$$

where $\dot{M}_{\rm c}$ is the planetesimal accretion rate, and $L_{\rm KH}$ is the luminosity of the atmosphere due to gas contraction obtained from our static model described in section 2. At the limit, $L_{\rm acc} = L_{\rm KH}$. For a given atmosphere model we can therefore estimate the maximum planetesimal accretion rate during the gas contraction phase in order for the atmosphere to be dominated by gas contraction. We choose as a fiducial case an atmosphere forming at 40 AU and with a core mass of $10M_\oplus$, described by a realistic equation of state. For this choice of parameters, the atmosphere crossover time is $t \sim 2.7$ Myrs, which is within the typical life time of a protoplanetary disk. The results are presented in Figure 10.

We label the resulting minimum core accretion rate as $\dot{M}_{\rm c,KH}$. The atmosphere growth rate $\dot{M}_{\rm atm}$ is also plotted for comparison. We therefore see that the core accretion rate has to be $\sim 2-3$ orders of magnitude lower than the atmosphere accretion rate for our assumptions to be valid. If the core had accreted planetesimals at this constant rate since it started forming, then the formation of a core massive enough to attract an atmosphere would not have been possible within typical disk life timescales, which indicates a slowing down of the planetesimal accretion regime. Possible explanations for that include the core having formed in the inner part of the disk and later migrated outwards, or the core having been depleted of planetesimals due to a giant neighbor. We also estimate the core accretion rate

$$\dot{M}_{\rm c,acc}(M_{\rm c}) \equiv \frac{M_{\rm c}}{\tau} \tag{12}$$

needed for the core to form on the same timescale as our model atmosphere, $\tau = 2.7$ Myrs, as well as a typical planetesimal accretion rate, for which the random velocities of the planetesimals are of the order of the Hill

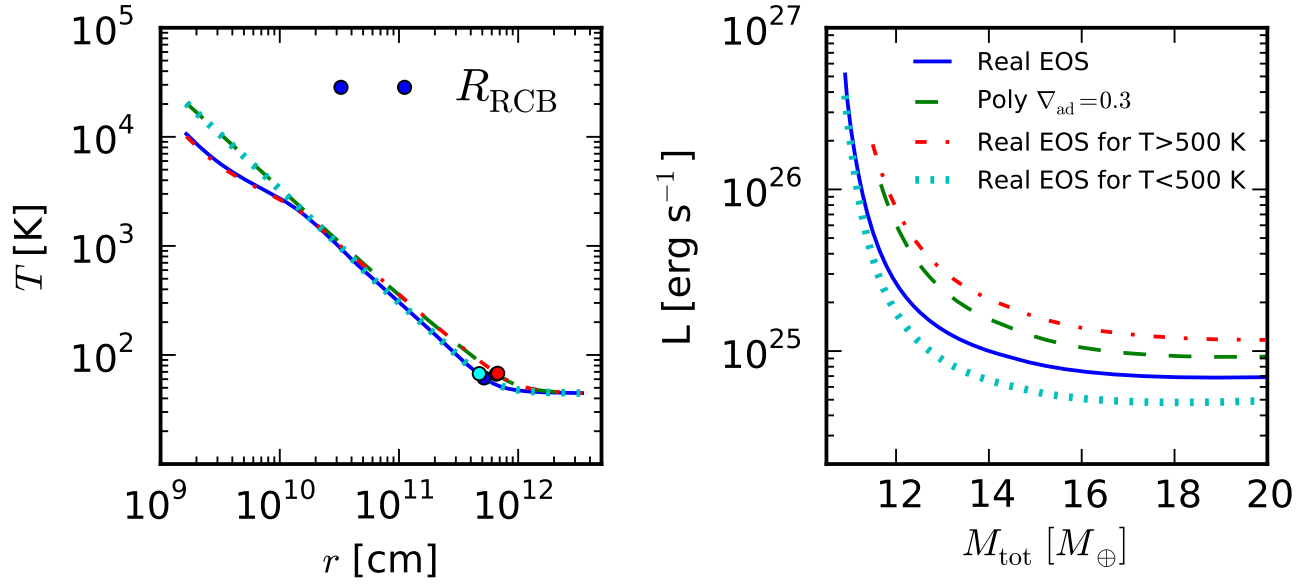

FIG. 6.— Left panel: Instantaneous emperature profile as a function of radius for a variety of EOS combinations, for a planet forming at 10 AU and with a fixed core mass $M_{\rm c} = 10M_\oplus$. The total mass (core + atmosphere) is $11.8M_\oplus$. The location of the radiative-convective boundary is marked. The effect of hydrogen spin isomers in the outer region of the atmosphere sets the location of the radiative-convective boundary. Right panel: Luminosity evolution as a function of total mass (core + atmosphere) for a variety of EOS combinations, for a planet forming at 10 AU and with a fixed core mass $M_{\rm c} = 5M_\oplus$. Dissociation deep in the atmosphere increases the luminosity when compared to an ideal gas polytrope, while the existence of the hydrogen spin isomers in the outer part of the atmosphere results in a lower luminosity. The two effects combined yield a lower luminosity for the realistic equation of state when compared to the polytrope.

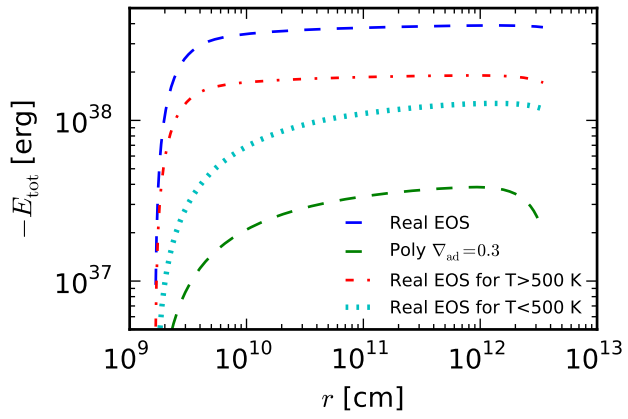

FIG. 7.— Instantaneous energy profiles as a function on radius for a variety of EOS combinations, for a planet forming at 10 AU and with a fixed core mass $M_{\rm c} = 10M_\oplus$. The total mass (core + atmosphere) is $11.8M_\oplus$. Hydrogen dissociation deep in the atmospheres causes the bulk of the energy to be concentrated at the bottom of the atmosphere.

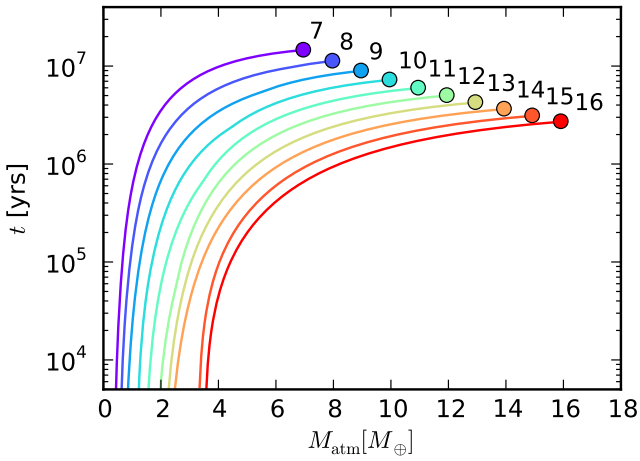

FIG. 8.— Time to grow an atmosphere of mass $M_{\rm atm}$ for cores with fixed masses between $7M_\oplus$ and $16M_\oplus$ at $a = 10$ AU in our fiducial disk. The circles mark the crossover time where $M_{\rm atm} \sim M_{\rm c}$. The numbers are labeling the core mass in Earth masses. A larger core mass results in a shorter crossover time.

velocity around the protoplanetary core (Goldreich et al. 2004). We denote this latter rate as $\dot{M}_{\rm c,typical}$. This is the accretion rate at the boundary between the dispersion dominated and shear dominated regimes. It is easy to see that $\dot{M}_{\rm c,typical}$ is more than one order of magnitude lower than the gas accretion rate of our model atmosphere $\dot{M}_{\rm atm}$, and lower than the core accretion rate $\dot{M}_{\rm c,acc}$ needed to grow the core and the atmosphere at the same time within the disk life time. As such, the formation of a giant planet by growing the core first, then letting the atmosphere cool is faster than growing the core and the atmosphere at the same time at a steady planetesimal accretion rate.

6.2. *Comparison with Standard Results*

Next, we are interested in whether hydrodynamic gas accumulation due to planetesimal accretion can already

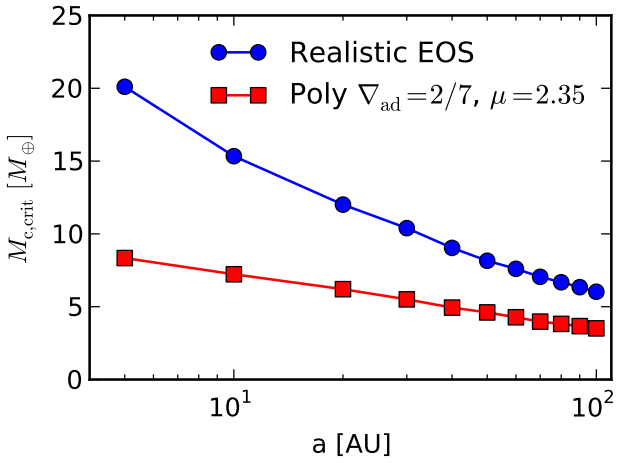

FIG. 9.— The minimum core mass for an atmosphere to initiate runaway gas accretion within the lifetime of a typical protoplanetary disk $t \sim 3$ Myrs as a function of semi-major axis, for a realistic hydrogen-helium mixture. The results of Piso & Youdin (in prep.) for an ideal diatomic gas are plotted for comparison. The realistic equation of state yields core masses larger by more than a factor of 2 when compared to the polytrope.

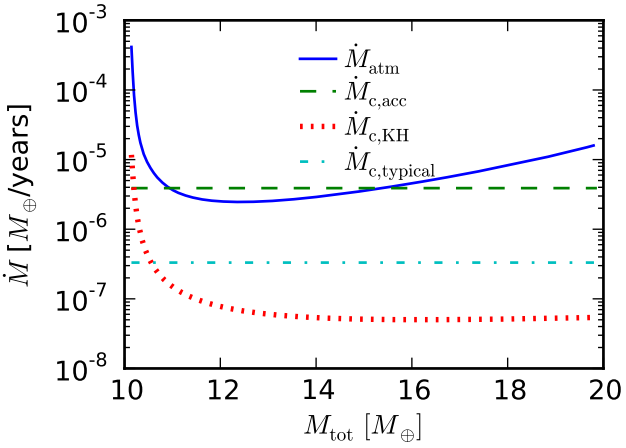

FIG. 10.— Various relevant accretion rates. $\dot{M}_{atm}$ is the growth rate of the atmosphere as estimated by our model, and $\dot{M}_{c,KH}$ is the maximum planetesimal accretion rate during the gas contraction phase in order for our regime to be valid. For comparison, we plot the core accretion rate $\dot{M}_{c,acc}$ necessary to grow the core on the same time scale as the atmosphere $\tau \sim 2.7$ Myrs, and a typical planetesimal accretion rate where the random velocity of the planetesimals is given by the Hill velocity due to the core.

commence before the atmosphere becomes unstable due to Kelvin-Helmholtz contraction, as our regime is no longer the relevant one under such conditions. A core that forms on the same timescale as our model atmosphere accretes planetesimals at a rate given by equation (12). This accretion rate is dependent on the core mass, which is steadily increasing. We therefore compare the critical core mass due to planetesimal accretion at this rate $M_{crit,acc}$ to the critical core mass as defined in our estimates $M_{c,crit}$ (see section 5). If $M_{crit,acc} < M_{c,crit}$, then the atmosphere has already initiated unstable gas accretion by the time Kelvin-Helmholtz contraction starts dominating.

In order to estimate the critical core mass due to planetesimal accretion $M_{crit,acc}$, we use the results of Rafikov (2006) for low luminosity atmospheres forming in the outer disk ($> 2-5$ AU), consistent with our region of interest. Rafikov (2006) assumes an ideal gas polytropic equation of state and a lower opacity than the standard ISM opacity that we use in our calculations (see equation 7), due to grain growth. In Piso & Youdin (in prep.) we showed that a reduction in opacity results in a shorter crossover time and therefore a lower critical core mass. In this section, we calculate the critical core mass for an ideal gas polytrope with the standard ISM opacity reduced by a factor of 100, which is comparable to the opacity law used by Rafikov (2006).

By relating his expression for the critical core mass to a given core mass dependent planetesimal accretion rate $\dot{M}(M_c)$, we find the following expression for the critical core mass when accretion luminosity dominates the evolution of the atmosphere:

$$M_{crit,acc} \sim \left[\frac{\dot{M}(M_c)}{64\pi^2 C}\frac{\kappa_0}{\sigma G^3}\frac{1}{R_c M_c^{1/3}}\left(\frac{k}{\mu}\right)^4\right]^{3/5}, \qquad (13)$$

with all the constants as defined in previous sections, and C a constant depending on the adiabatic gradient and disk properties (see Rafikov 2006, equation B3). We calculate $M_{crit,acc}$ for a range of core masses. The result is displayed in Figure 11.

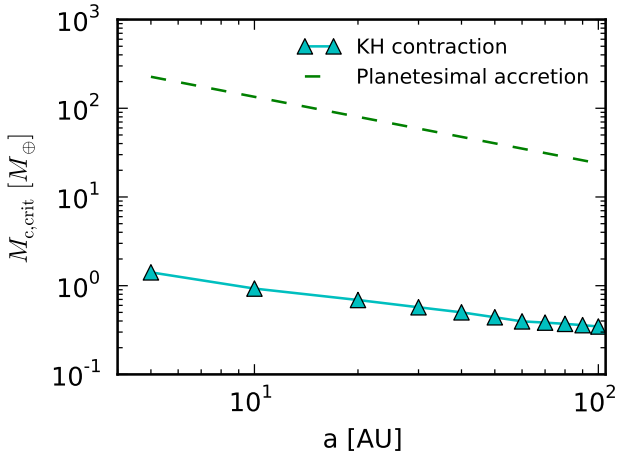

FIG. 11.— Comparison between the critical core mass $M_{crit,acc}$ due to planetesimal accretion and the assumed fixed core mass when gas contraction dominates, for a growth time of $\tau = 2.6$ Myrs. Our results yield lower core masses than in the standard case.

We see that the critical core mass due to planetesimal accretion is smaller than in the case in which planetesimal accretion dominates the evolution of the atmosphere. This brings us to two conclusions. First, we confirm that planetesimal accretion can be safely ignored in our regime of interest. Secondly, this comparison tells us that it is easier and more efficient to form a planet by growing the core first, then accreting a massive envelope, rather than by growing the core and atmosphere in

parallel. Moreover, our result represents a true, absolute minimum on the core mass that is needed to form a giant planet during the lifetime of the protoplanetary disk, as our core no longer grows.

As a final check, we investigate whether planetesimal accretion during the gas contraction phase at the rate $\dot{M}_{\rm KH}$ imposed by the condition that $L_{\rm acc} < L_{\rm KH}$ can alter the core mass enough to affect the time evolution of the atmosphere. We can quantitatively estimate the increase in core mass as

$$\Delta M_{\rm c} = \int_0^{t_{\rm crit}} \dot{M}_{\rm c} dt \approx \sum_i \dot{M}_{{\rm c}i} \Delta t_i, \tag{14}$$

where $t_{\rm crit}$ is the time elapsed until runaway gas accretion commences, and the accretion rate $\dot{M}_{{\rm c}i}$ is given by

$$\dot{M}_{{\rm c}i} = \frac{L_i R_{\rm c}}{G M_{\rm c}} \tag{15}$$

from equation (11), with L_i the luminosity of the atmosphere at time t_i in our model. For $M_{\rm c} = 10 M_\oplus$, we find $\Delta M_{\rm c} \approx 0.2 M_\oplus$. This mass increase is therefore negligible in comparison with the initial core mass. It follows that a significant increase in core mass that could potentially alter the time evolution of the atmosphere would occur on a longer time scale than the mass-doubling time for the unperturbed atmosphere. Therefore, the time evolution of the atmosphere is insensitive to core mass changes at a rate imposed by the assumption that $L_{\rm acc} < L_{\rm KH}$.

7. CONCLUSIONS

In this paper we have studied giant planet formation under the assumption that the planetesimal accretion rate is negligible and the atmosphere evolution is dominated by gas contraction. We have used the model developed in Piso & Youdin (in prep.) to build atmosphere profiles assuming that the nebular gas obeys a realistic equation of state that takes into account non-ideal effects. We found that the variations in the adiabatic index due to the realistic equation of state result in a significantly larger crossover time, and therefore critical core mass, when compared to an ideal gas polytrope. While for an ideal diatomic gas the minimum core mass to form a giant planet under the assumptions of our model is lower than the typically quoted value of $10 M_\oplus$ (see Piso & Youdin in prep.), the inclusion of non-ideal effects brings this values back to around $10 M_\oplus$,

We also compared our results to standard studies that assume that the evolution of the gaseous envelope is dominated by planetesimal accretion. We found that that our model yields lower core masses than the standard results. It is therefore easier to form a giant planet by growing the core first, then reducing the planetesimal accretion rate and let the atmosphere evolve on a Kelvin-Helmholtz time scale. Moreover, our results represent a true minimum on the core mass needed to form a giant planet during the typical lifetime of a protoplanetary disk.

REFERENCES

Bell, K. R. & Lin, D. N. C. 1994, ApJ, 427, 987
Bodenheimer, P. & Pollack, J. B. 1986, , 67, 391
Chiang, E. & Youdin, A. N. 2010, Annual Review of Earth and Planetary Sciences, 38, 493
D'Angelo, G., Durisen, R. H., & Lissauer, J. J. Giant Planet Formation, ed. S. Piper, 319–346
Farkas, A. 1935, Orthohydrogen, Parahydrogen and Heavy Hydrogen
Goldreich, P., Lithwick, Y., & Sari, R. 2004, ARA&A, 42, 549
Ikoma, M., Nakazawa, K., & Emori, H. 2000, ApJ, 537, 1013
Kippenhahn, R. & Weigert, A. 1990, Stellar Structure and Evolution
Kittel, C., Kroemer, H., & Landsberg, P. T. 1981, Nature, 289, 729
Mandl, F. 1989, Statistical Physics, 2nd Edition
Mizuno, H., Nakazawa, K., & Hayashi, C. 1978, Progress of Theoretical Physics, 60, 699
Papaloizou, J. C. B. & Terquem, C. 1999, ApJ, 521, 823
Rafikov, R. R. 2006, ApJ, 648, 666
Saumon, D., Chabrier, G., & van Horn, H. M. 1995, ApJS, 99, 713
Stevenson, D. J. 1982, Planet. Space Sci., 30, 755
Thompson, M. J. 2006, An introduction to astrophysical fluid dynamics
Wuchterl, G. 1993, , 106, 323

APPENDIX

EQUATION OF STATE TABLES

In this section we explain the procedure for extending and interpolating the Saumon et al. (1995) equation of state tables. The equation of state takes into account non ideal interactions, and includes physical treatments of dissociation and ionization. However, the Saumon et al. (1995) EOS tables only cover a relatively high range of temperatures and pressures: $2.10 < \log_{10} T({\rm K}) < 7.06$ and $4 < \log_{10} P({\rm dyn\ cm^{-2}}) < 19$. We consider cold disks, where the temperature and pressure drop to ~ 20 K and $\sim 10^{-4}$ dyn cm^{-2}, respectively (see equations (1b) and (2)). As such, it is necessary to extend the Saumon et al. (1995) EOS tables to lower temperature and pressure values.

We choose $\log_{10} T({\rm K}) = 1$ and $\log_{10} P({\rm dyn\ cm^{-2}}) = -4.4$ as our lower boundaries for temperature and pressure, respectively. Our temperature and pressure grid becomes: $1 < \log_{10} T({\rm K}) < 7.06$ and $-4.4 < \log_{10} P({\rm dyn\ cm^{-2}}) < 19$. The other thermodynamic variables in the tables are calculated as follows.

Hydrogen

For a system of particles, the partition function can be written as the product of all partition functions associated with each type of energy that the system can have:

$$Z = Z_t Z_r Z_v Z_e Z_n, \tag{A1}$$

where Z_t, Z_r, Z_v, Z_e and Z_n are the partition functions associated with translation, rotation, vibration, electronic excitation and nuclear excitation, respectively. For hydrogen, electronic and nuclear excitation are only significant at

temperatures higher than our region of interest ($\theta_e \approx 12000$ K and $\theta_n >> \theta_e$, where θ_e and θ_n are the characteristic temperatures for electronic and nuclear excitation, respectively). As such, we will only take into account the translation, rotation and vibration of the hydrogen molecule:

$$Z = Z_t Z_r Z_v \tag{A2}$$

The partition function associated with the motion of the center of mass of the molecule is given by (in the classical limit):

$$Z_t = (m/2\beta\pi\hbar^2)^{3/2} V, \tag{A3}$$

where $\beta = 1/(kT)$ and V is the volume. The rotational partition function is generally written as:

$$Z_r = \sum_0^\infty (2j+1) \exp\Big[\frac{-j(j+1)\Theta_r}{T}\Big], \tag{A4}$$

where Θ_r is the characteristic temperature for rotational motion. In the case of hydrogen, $\Theta_r \approx 85$ K. However, molecular hydrogen occurs in two isomeric forms: orthohydrogen, with the proton spins aligned parallel to each other, and parahydrogen, with the proton spins aligned antiparallel. Parahydrogen can only a have symmetric (even) wave function associated with rotation, while orthohydrogen can only have an antisymmetric (odd) wave function associated with rotation (see section 3 for an explanation why). The rotational partition functions for ortho- and parahydrogen can thus be written as:

$$Z_{\mathrm{r,para}} = \frac{1}{2} \sum_0^\infty (1 + (-1)^j)(2j+1) \exp\Big[-\frac{j(j+1)\Theta_r}{T}\Big] \tag{A5}$$

and

$$Z_{\mathrm{r,ortho}} = \frac{3}{2} \sum_0^\infty (1 - (-1)^j)(2j+1) \exp\Big[-\frac{j(j+1)\Theta_r}{T}\Big] \tag{A6}$$

The factor of 3 above accounts for the three-fold degeneracy of the ortho state.

When the two isomers are in equilibrium, the combined partition function is given by the sum of the individual partition functions, $Z_{\mathrm{r}} = Z_{\mathrm{r,ortho}} + Z_{\mathrm{r,para}}$ and can be written as:

$$Z_r = \sum_0^\infty (2 - (-1)^j)(2j+1) \exp\Big[\frac{-j(j+1)\Theta_r}{T}\Big] \tag{A7}$$

In our range of temperatures of interest, we found that Z_r converges after about 25 terms in the series.

Finally, the partition function for vibrational motion is given by:

$$Z_v = [1 - \exp(\theta_v/T)]^{-1}, \tag{A8}$$

where θ_v is the characteristic temperature for vibrational motion, $\theta_v \approx 6140$ K for hydrogen.

If the partition function of a system of N particles is known in terms of (V, T, N), the internal energy and entropy of the system can be determined as follows:

$$U_N = kT^2 \Big(\frac{\partial \log Z}{\partial T}\Big)_{V,N} \tag{A9}$$

$$S_N = k \log Z + \frac{U_N}{T} \tag{A10}$$

The energy, and entropy per mass and specific heat capacity will subsequently be:

$$U = \mathcal{R}T^2 \Big(\frac{\partial \log Z}{\partial T}\Big)_{V,N} \tag{A11}$$

$$S = \mathcal{R} \log Z + \frac{U}{T} \tag{A12}$$

$$C_v = \Big(\frac{\partial U}{\partial T}\Big)_{V,N} \tag{A13}$$

Since $Z = Z_t Z_r Z_v$, it is easy to notice that $U = U_t + U_r + U_v$ and $S = S_t + S_r + S_v$, where U_t, U_r, U_v, S_t, S_r, S_v are the quantities corresponding to the individual translation, rotation and partition functions, respectively.

It can be shown that the entropy per mass due to translational motion can be expressed as:

$$S_t = \mathcal{R}\Big[\frac{5}{2}\ln T - \ln P + \ln\Big(\frac{(2\pi)^{3/2}\mathcal{R}^{5/2}\mu^4}{h^3}\Big) + \frac{5}{2}\Big] \tag{A14}$$

with μ the mean molecular weight. Equation (A14) is known as the Sackur-Tetrode formula, and it is only applicable to an ideal gas. It can also be easily shown that the internal energy per mass due to translational motion is given by:

$$U_t = \frac{3}{2}\mathcal{R}T \tag{A15}$$

Putting all of the above together, we can now evaluate the thermodynamic quantities needed to extend the Saumon et al. (1995) EOS tables to low temperatures and pressures.

1. **Density.** In the low temperature, low pressure regime, hydrogen is molecular and behaves like an ideal gas. As such, the density in this region follows the ideal gas law $P = \rho\mathcal{R}T$.

2. **Internal energy per mass.** $U = U_t + U_r + U_v$, where U_t is given by equation (A15), and U_r, U_v are determined using equations (A11), (A7) and (A8) above.

3. **Entropy per unit mass**. Similarly, $S = S_t + S_r + S_v$, where S_t is given by equation (A14), and S_r, S_v can be determined from equation (A12) and the calculated expressions for U_r and U_v, respectively.

4. **Entropy logarithmic derivatives**. The logarithmic derivatives S_T and S_P are given by:

$$S_T = \frac{\partial \log S}{\partial \log T}\Big|_P \tag{A16}$$

and

$$S_T = \frac{\partial \log S}{\partial \log P}\Big|_T \tag{A17}$$

We calculate S_T and S_P using the table values for S, T and P, and a linear central difference formula.

5. **Adiabatic gradient** ∇_{ad}. The adiabatic gradient is defined as:

$$\nabla_{ad} = \frac{\partial \log T}{\partial \log P}\Big|_S = -\frac{S_P}{S_T} \tag{A18}$$

We evaluate it from the tabulated values for S_T and S_P determined above. Figure 1 shows a contour plot of the adiabatic index for the extended EOS table, while the black lines represent constant entropy curves. The upper right part of the plot ($\log T > 2.1$ and $\log P > 4$) is based on the Saumon et al. (1995) EOS table, while the rest of the plot is our extension. We see that the two tables join smoothly for entropy curves between $8.80 < \log S(\mathrm{K\ g^{-1}}) < 9.07$.

Helium

We extend the helium EOS tables based on a similar procedure. Since helium is primarily neutral and atomic at low temperatures and pressures, we treat it as an ideal monoatomic gas, and subsequently only take into account the translational components of the necessary thermodynamic quantities (see subsection A.1 above for details). The analogous ∇_{ad} contour plot for helium can be seen in Figure 2. We notice that, in the case of helium, the original and extended table join smoothly for entropy curves between $8.29 < \log S(\mathrm{K\ g^{-1}}) < 8.77$.

Lastly, we obtain the equation of state tables for the hydrogen-helium mixture thorough the procedure described in Saumon et al. (1995), for a helium mass fraction $Y = 0.3$.

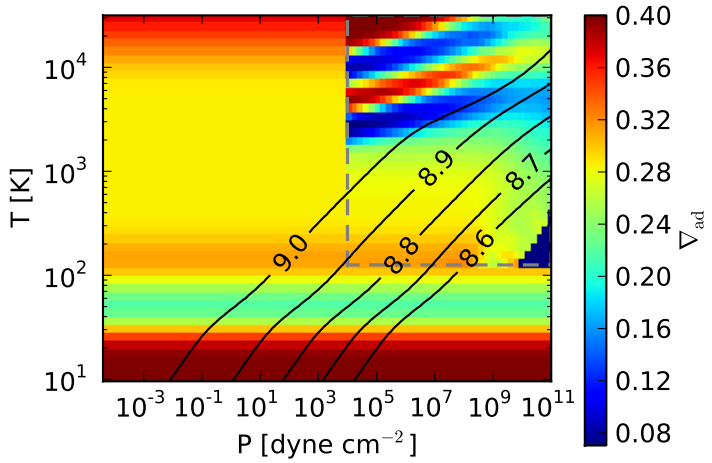

FIG. 12.— Contour plot of the adiabatic gradient ∇_{ad} for the hydrogen extended table. The black curves represent constant entropy curves.

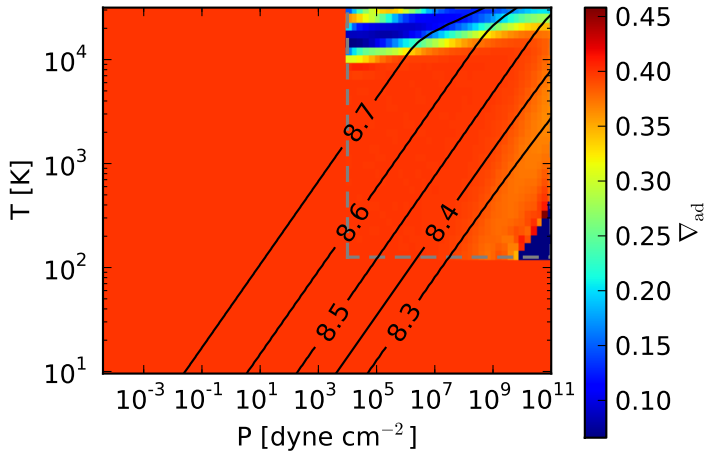

FIG. 13.— Contour plot for the adiabatic gradient ∇_{ad} for the helium extended table. The black curves represent constant entropy curves.

ADIABATIC GRADIENT DURING PARTIAL IONIZATION

For a partially ionized gas, the total internal energy includes contributions from the individual internal energies of neutral atoms, ions and electrons, as well as from the ionization energy. Specifically, if we denote the internal energies of neutral hydrogen, protons and electrons as U_H, U_+ and U_e, respectively, then the total internal energy of the gas is given by:

$$U = U_H + U_+ + U_e + x\chi, \tag{B1}$$

where x is the ionization fraction and χ is the ionization energy (equal to -13.6 eV for hydrogen). The ionization fraction can be determined from the Saha equation (see e.g., Kippenhahn & Weigert 1990).

$$\frac{x^2}{1-x}\frac{\rho}{m_H} = \frac{(2\pi m_e k_B T)^{3/2}}{h^3} e^{-\chi/k_B T}, \tag{B2}$$

where m_e is the mass of the electron and h is Planck's constant. It can be seen from the Saha equation that the ionization fraction depends only on the gas temperature and density: $x = x(T, \rho)$. As such, all the thermodynamic quantities also depend only on the gas temperature and density, and hence on the equation of state. The adiabatic gradient is given by (see Kippenhahn & Weigert 1990, chapter 14 for a derivation):

$$\nabla_{\rm ad} = \frac{2 + x(1-x)\Phi_H}{5 + x(1-x)\Phi_H^2}, \tag{B3}$$

with $\Phi_H = \frac{5}{2} + \frac{\chi}{kT}$. Figure 14 shows the behavior of $\nabla_{\rm ad}$ for partially ionized hydrogen. We recover $\nabla_{\rm ad} = 2/5$ for $x = 0$ (pure atomic hydrogen) and $x = 1$ (fully ionized plasma). The adiabatic gradient decreases significantly for intermediate values of x, becoming smaller than 0.1 at its minimum (for $x = 0.5$).

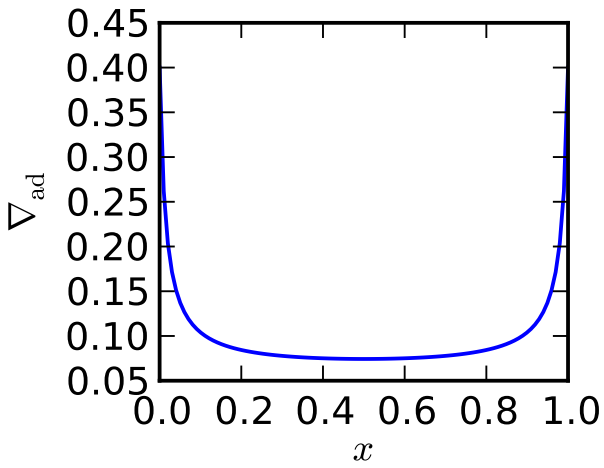

FIG. 14.— Adiabatic gradient as a function of the hydrogen ionization fraction x. The adiabatic gradient is $\nabla_{\rm ad} = 2/5$ for pure atomic hydrogen ($x = 0$) and fully ionized hydrogen ($x = 1$), and drops to low values during partial ionization.